

**BOUNDARY ELEMENT METHOD PREDICTIONS OF THE INFLUENCE OF
THE ELECTROLYTE ON THE GALVANIC CORROSION OF AZ91D
COUPLED TO STEEL**

Jimmy X. Jia, Guangling Song, Andrej Atrens

CRC for Cast Metals Manufacturing (CAST), Division of Materials,
School of Engineering, The University of Queensland, St Lucia, QLD 4072, Australia

ABSTRACT

This research investigated the galvanic corrosion of the magnesium alloy AZ91D coupled to steel. The galvanic current distribution was measured in 5% NaCl solution, corrosive water and an auto coolant. The experimental measurements were compared with predictions from a Boundary Element Method (BEM) model. The boundary condition, required as an input into the BEM model, needs to be a polarization curve that accurately reflects the corrosion process. Provided that the polarization curve does reflect steady state, the BEM model is expected to be able to reflect steady state galvanic corrosion.

Keywords : Magnesium alloys; Galvanic corrosion; Boundary element method

INTRODUCTION

The study of the galvanic corrosion of magnesium is becoming increasingly important as the use of magnesium increases rapidly in the auto and aerospace industries due to their lightweight advantages. However, the corrosion of magnesium is one of the main concerns that limits the application of magnesium in industry [1, 2]. Corrosive attack may occur via a number of different mechanisms. But galvanic corrosion is probably the most important for magnesium because magnesium is the most anodic structural metal and consequently corrodes preferentially when joined

to the other common metals of construction, such as aluminum or steel [3]. Therefore, the design of many industrial projects are directly determined by galvanic corrosion.

In order to be able to predict the galvanic corrosion in various structural components during the design process, it is first necessary to understand (1) the galvanic corrosion of magnesium alloys in different corrosive environments, and (2) the potential challenges in using a computing method to simulate the galvanic corrosion distribution in order to provide a detailed quantitative analysis for real conditions. The work presented in this paper has been undertaken as part of an experimental program examining the Boundary Element Method (BEM) program BEASY for the prediction of galvanic corrosion.

Prior studies of galvanic corrosion of magnesium have been scarce. The earliest study, started in the 1950s by Teeple [4], investigated the influence of location and climate. This study revealed that the galvanic corrosion rate of magnesium varied with location of atmospheric exposure. Different locations produced different corrosion rates because of the different electrolyte properties of the condensed film on the metal surface [4]. Galvanic corrosion could be detrimental for magnesium in one environment while it was almost harmless in another environment. This has provided industry with helpful information to select magnesium for an appropriate environment. However, the study was time consuming. It is often not practical to wait years to have the test results for each particular service environment.

Limited studies have addressed the effect of electrolyte on the galvanic corrosion of magnesium. More effort has been focused on general corrosion and particularly on the influence of the ion species in solution and the influence of cathodic impurity elements in the alloy on the general corrosion rate for magnesium alloys [5-13]. The influence of the electrolyte involves many factors such as pH, composition, concentration of the ions and the conductivity of the electrolyte. The influence of conductivity on galvanic corrosion has been studied in terms of “macroscopic” and “microscopic” galvanic cells [14], or in terms of the Wagner number [15, 16]. Recent research

revealed the complicated “alkalization”, “passivation” and “poisoning” effects during the salt spray exposure which maybe difficult to predict accurately using numerical methods [3]. The present study investigated the galvanic corrosion of magnesium alloy AZ91D in sodium chloride solution, standard corrosive water and a commercial coolant. The three media were chosen to represent highly corrosive, medium corrosive and corrosion inhibited environments.

Various measurement methods have been employed to measure galvanic corrosion. Galvanic corrosion of magnesium has been measured in terms of weight loss and pitting depth [4, 17-21]. The weight loss and pitting depth methods actually measure the total corrosion rate which is the sum of general and galvanic corrosion. These methods are not accurate in terms of just the galvanic corrosion. The method of surface potential scanning provides the potential distribution measurement [22], but the potential is not directly related to the galvanic corrosion rate. The present study measured the galvanic current which directly relates to the galvanic corrosion rate.

The BEM is a relatively new and particularly promising numerical method and is becoming more important with recent developments in computer technology. Numerical methods have been utilized in galvanic corrosion analysis since the early 1980's. The application of BEM in galvanic corrosion analysis has been reviewed by Adey and Niku [23], Munn [24], Aoki [25, 26] and Brebbia [27]. Adey [23] stated that BEM was suitable for modeling corrosion, and that computer simulation of galvanic corrosion could be undertaken with confidence with programs like BEASY. Our preliminary research [28] showed that the BEM program BEASY provided calculated values in agreement with analytical approaches and FEM calculations. Most of the previous studies have also reported agreement between the modeling predictions and the experimental measurements for the galvanic current distribution [25, 26, 29-36]. In contrast, Ault and Meany [37] concluded: a) “the deepest pit was not immediately adjacent to the cathodic metals that most mathematical models predict”; b) “the mathematical model only can provide a order of magnitude estimation of galvanic current flow”; c) “the mathematical model can neither accurately predict long term current distribution nor the magnitude of pitting corrosion”. These conclusions are of particular significance

for the present study on the galvanic corrosion of magnesium because localized corrosion is often the form of corrosion of magnesium in practical solutions as typified by 5% NaCl solution. Thus further evaluation of BEM is necessary to reveal the potential challenges in the prediction of galvanic corrosion of magnesium using BEM and to understand the discrepancies between mathematical prediction and experimental results.

In this study, the environment was taken into account using the experimentally measured polarization curve as the boundary condition. The results of the numerical analysis were compared with the experimentally measured galvanic current. The aim of this study was to provide insight into galvanic corrosion prediction and galvanic corrosion prevention for real auto, aerospace or marine components.

EXPERIMENTAL PROCEDURE

Galvanic corrosion Assembly

The high pressure die cast (HPDC) magnesium alloy AZ91D and mild steel were used in this study. AZ91D was chosen because it is the most widely used magnesium alloy. AZ91D contains about 9% aluminium and less than 1% zinc. Mild steel is the metal most used in industry [38]. The metal plates were molded in epoxy as shown in Fig. 1. The insulation distance was 0.5mm between adjacent plates. The galvanic current was measured for six plates of AZ91D and six plates of mild steel. The surface area exposed to the solution of each metal plate was 1.2 mm (thickness) X 35 mm (width) (42 mm^2 surface area). The galvanic cell size could be changed by connecting or disconnecting some of the metal plates. The solution depth was arbitrarily chosen as 10 mm throughout this study.

Electrolytes

5% NaCl solution, corrosive water and a commercial coolant were used. The 5% NaCl solution represents a severe corrosive environment such as a marine environment or the environment near the beach. The corrosive water simulates a less aggressively corrosive environment, and the coolant was chosen to represent an inhibitive or protective environment. The conductivities were measured using

a platinum conductivity cell to be 79500 $\mu\text{S}\cdot\text{cm}$, 698 $\mu\text{S}\cdot\text{cm}$ and 451 $\mu\text{S}\cdot\text{cm}$ for the 5% NaCl solution, corrosive water and coolant respectively. The 5% NaCl solution and the corrosive water were made with analytical reagents and deionized water. The corrosive water was made up according to the ASTM standard D1384 and had the following composition: 148 mg Na_2SO_4 , 165 mg NaCl and 138 mg NaHCO_3 in 1 liter of solution [39]. The commercial coolant contained 33% of ethylene glycol, demineralised water and proprietary corrosion inhibitors and is marketed by Mobil as “Coolant 33 Plus”.

Galvanic Current Measurement

The surface of the electrodes of the specimen was polished by 1200# silicon sandpaper, washed with water and ethanol and dried. The specimen was immediately immersed in the solution. A multi-channel Zero Resistance Ammeter (ZRA) was used to measure the galvanic currents passing through each electrode as a function of time as illustrated in Fig. 1.

Polarization Curve Measurement

Fig. 2 presents the experimental arrangement for the measurement of the potentiodynamic and galvanostatic polarization curves. The measurement of galvanostatic polarization curves used the potentiodynamic curves as a guide for the current density values. For each applied constant current density, the potential was measured with time to give the galvanostatic polarization curves at 5 to 10 minutes for the 5% NaCl solution, at 3 to 4 hours for corrosive water and at 3 to 4 hours and 12 hours for the coolant. The solartron 1287 electrochemical interface was used to measure the polarization curves using an Ag/AgCl reference electrode. The solution resistance was measured using the 1255B Frequency Response Analyzer and all polarization curves have been corrected for the potential drop caused by the solution resistance.

BEM model

The mathematical formulation has been described by Adey [23] for a uniform, isotropic electrolyte domain Ω as illustrated in Figure 3. For a uniform, isotropic electrolyte system in steady state, the

potential obeys the Laplace equation:

$$\nabla^2 \phi = 0, \quad (1)$$

The Laplace equation is solved using the following boundary conditions:

$$\phi = \phi_0, \quad \text{on } \Gamma_1, \quad (2)$$

$$I = I_0, \quad \text{on } \Gamma_2, \quad (3)$$

$$I_a = -f_a(\phi), \quad \text{on } \Gamma_{3a}, \quad (4)$$

$$I_c = -f_c(\phi), \quad \text{on } \Gamma_{3c}, \quad (5)$$

where $\Gamma (\equiv \Gamma_1 + \Gamma_2 + \Gamma_{3a} + \Gamma_{3c})$ is the entire surface of the electrolyte domain Ω , I is the current density across the boundary, and ϕ is the potential, ϕ_0 and I_0 are given constant values of potential and current density respectively. For the current research, there was no region Γ_1 of applied potential, and the $I = 0$ applied for all regions other than the AZ91D and steel electrodes in figure 1. $f_a(\phi)$ and $f_c(\phi)$ are linear or non-linear functions that describe the anode and cathode electrode kinetics respectively.

The boundary integral equations for all elements can be assembled into a system of linear simultaneous equations, which is expressed in a matrix form as follows

$$H\phi = GI \quad (6)[23]$$

where H and G are problem influence matrices, and ϕ and I represent potential and current density vectors respectively.

The size of the equation system is defined by the number of nodes. Partitioning the ϕ and I into those nodes which form the anode and the cathode regions and applying the boundary condition of equation (4) and equation (5), gives

$$\begin{bmatrix} h_{aa} & h_{ac} \\ h_{ca} & h_{cc} \end{bmatrix} \begin{bmatrix} \phi_a \\ \phi_c \end{bmatrix} = \begin{bmatrix} g_{aa} & g_{ac} \\ g_{ca} & g_{cc} \end{bmatrix} \begin{bmatrix} f_a(\phi_a) \\ f_c(\phi_c) \end{bmatrix} \quad (7)[23]$$

where $\begin{bmatrix} h_{aa} & h_{ac} \\ h_{ca} & h_{cc} \end{bmatrix}$ and $\begin{bmatrix} g_{aa} & g_{ac} \\ g_{ca} & g_{cc} \end{bmatrix}$ are elements of the problem influence matrices, $\begin{bmatrix} \phi_a \\ \phi_c \end{bmatrix}$ and

$\begin{bmatrix} f_a(\phi_a) \\ f_c(\phi_c) \end{bmatrix}$ are the polarization curves. Equation (6) was then solved by the iterative method, the

Newton-Raphson method .

In this study, the non-linear relationships between potential and current density equation (4) and (5) were determined as the experimentally measured polarization curves for the AZ91D and steel elements. The model geometry was created in the BEASY environment in which the boundary was divided into 80 AZ91D elements and 80 steel elements as illustrated in figure 4.

The boundary element program BEASY was used to implement the BEM. The input parameters included the physical geometry of the galvanic couple, the electrolyte

conductivity and the boundary conditions of $\begin{bmatrix} \phi_{a0} \\ \phi_{c0} \end{bmatrix}$ and $\begin{bmatrix} f'_a(\phi) \\ f'_c(\phi) \end{bmatrix}$, where ϕ_{a0} was the

open circuit potential of the anode; ϕ_{c0} was the open circuit potential of the cathode;

$f'_a(\phi)$ was the function used in BEASY to represent the anode metal polarization curve

given by equation (4); similarly $f'_c(\phi)$ is the function representing the cathode metal

polarization curve. The functions $f'_a(\phi)$ and $f'_c(\phi)$ were defined using the piecewise

linear approach. The polarization curve was divided into small segments, such that for

each segment there was a linear relationship between the potential and current given by:

$$I = f(\phi) = k(\phi - \phi_a) + I_a \quad (8)$$

where k , ϕ_a and I_a were known constants for each line segment.

RESULTS

Polarization Curves

Potentiodynamic polarization curves of AZ91D and steel were reproducible in all three solutions.

For example, figure 5 presents four repeated measurements for AZ91D and steel in the 5%NaCl solution using a scan rate of 2 mV/s. The repeated measurements showed a reasonable agreement. The polarization curves Fig. 6 presents typical potentiodynamic polarization curves for the three solutions.

The shape of polarization curve can be influenced by a corrosion product film which seems to have been significant for AZ91D in the coolant. Figure 7 presents polarization curves for AZ91D measured using decreasing potential scan rates. As the scan rate decreased from 2 mV/s to 0.6 mV/min, there was a passive range in the polarization curves, the current in the passive range decreased from 4×10^{-4} A/cm² at 2 mV/min to 2×10^{-4} A/cm² at 0.6 mV/min, and the open circuit potential shifted in the anodic direction from -1.75 V at the scan rate of 2 mV/s to -1.52 V at the scan rate of 0.6 mV/min. This passivity could be caused by an increasingly protective surface film. The different scan rate could reflect the influence of different thickness of the deposited film. A slower scan rate allows more time for the film to grow and could result in a thicker film which could provide stronger protection.

The galvanic current density of equal areas of AZ19D and steel can be estimated from the intersection of the superimposed polarization curves of AZ91D and steel. This method is useful in providing a qualitative estimation but it does not provide the exact galvanic corrosion rate [41]. The polarization behavior of AZ91D and steel were quite different in 5%NaCl solution, corrosive water and coolant. Figure 6 illustrates the polarization curves for AZ91D and steel in 5%NaCl solution, corrosive water and coolant measured with the scan rate of 2 mV/second. These curves indicate that the biggest coupled galvanic current density would be expected in 5%NaCl solution and the smaller coupled galvanic current would be expected in corrosive water. The coupled current densities would be expected to be quite similar in value in the coolant and corrosive water.

Hack and Scully [40] indicated that it was necessary to use long-term polarization curves to adequately predict the galvanic corrosion, and as a consequence, galvanostatic curves were

measured. The particular current density values, chosen based on the potentiostatic polarization curves, were applied and the resulting potential was measured as shown by typical curves in figures 8 to 13. In each case, multiple measurements were made. The potential of AZ91D and steel rapidly reached steady state values in the 5%NaCl solution as shown in figures 8 and 9. Intense hydrogen evolution on the surface of steel and AZ91D stirred up the corrosion product inside the solution and there was no stable deposited film on the surface of AZ91D. In contrast, approach to steady state was much slower in corrosive water and mobile coolant. The hydrogen evolution rate was much slower than that in 5% NaCl solution. Therefore it could become a bit easier for a corrosion product film to form on the surface of AZ91D. Galvanostatic polarization curves were derived at 5 to 10 min for 5%NaCl as shown in figure 14, 3 to 4 hour for corrosive water as shown in figure 15 and 3 to 4 hours and 12 hours for coolant as shown in figure 16.

For the 5% NaCl solution, approach to steady state was rapid, steady state had been reached by 5 to 10 min, whereafter there was little further change. Consequently the polarization curves represent steady state and thus maybe used as the boundary conditions for the BEM model to predict steady state galvanic corrosion. this is of significance when considering steady state for the galvanic corrosion measurements, and particularly figure 19.

There was some initial variation in the potential of steel in corrosive water, but the potential was essentially constant after 2 hours (figure 10). In contrast, the potential of AZ91D increased steadily for lower values of the polarization current below 0.072 mA/cm^2 (figure 11). This could be due to the deposition of a corrosion product film which had some protective character [42]. But the potential of AZ91D appeared to approach a steady state value rapidly when the applied current density exceeded 0.072 mA/cm^2 .

Figures 12 and 13 show typical curves for potential versus time in the coolant. The potential of the AZ91D continued to change even after twelve hours whereas the potential of the steel seemed to have begun to stabilize by about 6 hours. The change in potential is interpreted to be due to

formation of the deposition of a film on the electrode surface. The interpretation of the oscillations of the potential on the AZ91D electrode is uncertain. The shape of the oscillation is different to that expected to be associated with film formation and local break down of the surface film.

Figure 14, 15 and 16 show the galvanostatic polarization curves compared with the potentiodynamic polarization curves for AZ91D and steel in the 5%NaCl solution, corrosive water and coolant. The data for the two methods were within experimental error, but nevertheless there were significant differences in the shapes of the curves. The largest difference in polarization curve shape occurred in coolant which is attributed to the approach to steady state, the influence of inhibitors or the protective deposition film on the electrode surface. The least difference in polarization curve shape occurred in 5% NaCl solution due the rapid attainment of steady state because there was no formation of a protective deposition film on the electrodes surface and thus less interference occurred. None of the polarization curves from either method can be certain to be exactly representative of the real situation experienced by the AZ91D-steel galvanic couple. This is because the AZ91D and steel of the galvanic couple did not experience an exactly constant current density or constant potential. Furthermore, films or inhibitors adsorbed maybe different under potentiodynamic and galvanostatic polarization conditions.

Galvanic Current Measurements

The measurement of galvanic current for electrodes of AZ91D and steel in 5% NaCl solution, corrosive water and coolant are shown in figures 17 to 25. In the 5% NaCl solution, galvanic currents of electrodes AZ91D1 to AZ91D3 exhibited relatively constant high values whereas the galvanic currents of electrodes AZ91D 4 to AZ91D 6 initial decreased and then approach steady state values as shown in figure 17. This initial decrease is interpreted as a result of the corrosion product deposit contributing some protection on electrodes of Mg 4 to Mg 6, but there was little protection on electrodes Mg 1 to Mg 3 which suffered intense dissolution. The current in the steel electrodes also decreased slightly as shown in figure 18. The total current from the AZ91D electrodes (positive) should be equal to that from the steel electrodes (negative). The sum of the total

current from the AZ91D and steel oscillated around the zero as shown in figure 19. There was an initial transient, whereafter the sum of the total current gradually tended to be stable around zero as the galvanic corrosion became stabilized.

In corrosive water, the galvanic current for the AZ91D and steel electrodes also changed somewhat with time as shown in figures 20 and 21. The current of the steel electrodes was relatively stable (figure 20). The current of electrodes Mg 1 to 3 changed slightly with time whilst the current on electrodes Mg 4 to 6 oscillated a little. The sum of the total current from the AZ91D and steel during the galvanic current measurement tended to oscillate around zero when the galvanic corrosion became stabilized as shown in figure 22.

The galvanic current was relatively evenly distributed and decreased simultaneously and evenly with time on all AZ91D electrodes in the coolant as shown in figure 23. This is interpreted as due to the inhibitors in the coolant causing a significant reduction in both general corrosion and galvanic corrosion. The current of Mg 1 and 2 electrodes, close to the steel electrodes, exhibited current values lower than that of the other AZ91D electrodes. This is interpreted as due to the inhibiting effect being greater with a higher initial Mg^{2+} concentration in the coolant. The current on the steel electrodes decreased with time and decreased with increasing distance from the AZ91D-steel interface as shown in figure 24. The sum of the total current from the AZ91D and steel was close to zero in the coolant system as shown in 25.

Surface After Galvanic Corrosion

Figures 26 to 28 show the surface of the AZ91D-steel galvanic couple after the galvanic corrosion test in the three solutions. In the 5% NaCl solution (figure 26), there was severe pitting on the surface of the AZ91D electrodes with the pitting being severest for electrode Mg 1. The corrosion product was stirred up in the solution by the intense hydrogen revolution. There was no obvious deposit film on the surface of the AZ91D and steel electrodes. In corrosive water (figure 27), there were large pits in the Mg 1 and Mg 2 electrodes, the rest of the AZ91D electrodes exhibited only

slight pitting with a few small pits randomly distributed on the surface of each electrode. There was corrosion product deposited on the surface of the steel electrodes which formed a very loose porous layer. In the coolant (figure 28), there was no obvious pitting on the surface of all the AZ91D electrodes. There were only a few small pit along the edge of the Mg 1 electrode adjacent to the AZ91D-steel interface. The surface appearance could be interpreted in terms of a fine deposit film on the surface of all AZ91D electrodes; but could also be interpreted in terms of changes in surface reflectivity due to changes in surface topography.

Comparison of Model Calculations with the Experimental Measurements

The results of the BEM model simulating the galvanic corrosion in 5% NaCl solution, corrosive water and coolant environments are compared with the experimental measurements in figures 29, 30, 31 and 32.

For the 5% NaCl solution, the boundary conditions used are presented in Table 1. There was reasonably good agreement between the experimental measurement and the BEM calculation of the galvanic currents for both the AZ91D and steel electrodes as shown in figure 29. For this case, there was a good agreement between the galvanostatic and potentiostatic polarization curves. And there was steady state in the measurement of the galvanicstatic polarization curves and for the galvanic current measurements. This indicates that the BEM model is capable of an adequate prediction provided that the BEM model has an appropriate boundary condition as input. That is the BEM model needs a polarization curve that adequately reflects the corrosion behavior taking place at the surface.

In corrosive water, the boundary conditions used are presented in Table 2. There was good agreement between the experimental measurements and the BEM model prediction for the steel electrodes, but only moderate agreement for electrodes Mg 1 to 4 when the current was equal to or higher than 0.072 mA.cm^2 . However, there was a large difference between the experimental measurement and the BEM model prediction for electrodes AZ91D 5 and 6 when the currents was

less than 0.072 mA/cm^2 . This indicated that the BEM prediction tended to overestimate the galvanic current at the same distance from the AZ91D-steel interface which may be due to the formation of a corrosion product film. It is possible that film formation has different kinetics during the measurement of galvanostatic polarization curves and the measurements of galvanic currents. There is some evidence in support of such a film in the decrease of the galvanic current observed for AZ91D electrodes (figure 20). A more important deduction is that the BEM model did not have an appropriate boundary condition as input. That means that the measured polarization curve was inadequate for low current values. This was the part of the galvanostatic polarization curve where steady state had not been reached.

The influence of the variations in the measured galvanic polarization curves was explored by using the various polarization curves as documented in table 1 and 2 as input to the BEM model. The results of the BEM calculations are presented in figure 29 and 30. There was only a small variation among those modeling results in 5% NaCl solution (figure 29) and there was almost no difference among those modeling results in corrosive water (figure 30). This indicated that the experimental error during the polarization measurement did not contribute a significant error to the BEM calculations.

For the coolant, the BEM model prediction for the galvanic current on the AZ91D electrodes with the galvanostatic polarization curve as input boundary conditions did not agree with the experimental measurement as shown in figure 31. The curve 4h represents the model prediction using the galvanostatic polarization curve derived at 4 hours as the boundary condition and the curve 12h represents the model prediction using the galvanostatic polarization curve derived at 12 hours as boundary condition. There was no agreement between the experimental measurements and the BEM calculations with the time dependent galvanostatic polarization curve as the boundary conditions. The calculation did predict that the galvanic current decreased with time using the polarization curve measured at 4 hours and 12 hours immersion test (4h and 12h) as shown in figure 31, but there was no agreement in the galvanic current distribution or the value of the current. This leads to the

conclusion that the galvanostatic polarization curve was not representative of the behavior of AZ91D in the coolant. The galvanostatic polarization curve measurements had not reached steady state, so there may be a significant difference between the measured galvanostatic polarization curve and the “true” polarization curve. Furthermore, there was a significant gap in the galvanostatic curve/data in the current range between 0.00 and 0.39 mA/cm², and also there was a significant difference in the curve shapes in this range between the galvanostatic and potentiostatic polarization curves. The AZ91D electrodes experienced a continuous decrease in galvanic current in the galvanic current measurement. The AZ91D in the coolant for the real galvanic corrosion situation did not experience a constant current or constant potential polarization but a gradually decreasing current which was attributed to the growth of the deposit film. The unrealistic boundary condition is thought to be the cause of the disagreement between the BEM calculations and experimental measurement.

In contrast, the BEM calculation using the slow scan rate potentiodynamic polarization curve as the boundary conditions did show some agreement with the experimental measurements as shown in figure 32. BEM-PD1 was the BEM calculation using the potentiodynamic polarization curve for AZ91D measured with the scan rate of 2 mV/min as the boundary condition and BEM-PD2 was the BEM calculation using the potentiodynamic polarization curve measured with the scan rate of 0.6 mV/min as the boundary condition. The galvanic current predicted by BEM-PD1 showed an agreement with the initial measured galvanic current. The calculated current in BEM-PD2 showed a decreased galvanic currents for the AZ91D electrodes at the AZ91D-steel interface, thus providing a current density distribution somewhat similar to that measured. The different potential scan rates reflected the influence of the deposit film growth on the galvanic corrosion and thus gave an improved prediction of galvanic current development on AZ91D electrode. Nevertheless, the potential dynamic polarization curve still did not provide the exact relationship between galvanic current and time.

Discussion

In 5% NaCl solution, the galvanic current was reasonably predicted by BEM based BEASY program for the AZ91D-steel couple. 5%NaCl solution is an aggressive environment and intense hydrogen evolution stirred up the corrosion product. The galvanic corrosion of AZ91 in 5% NaCl solution was unlikely to be interfered by the formation of a surface film. The galvanostatic polarization curve of AZ91D in 5% NaCl solution rapidly approached steady state, was in good agreement with the potentiodynamic polarization curve and was likely to be representative of the galvanic corrosion behavior of the AZ91D.

In contrast, in the coolant, there was no trend agreement between the experimental measurement and the calculated galvanic current distribution using the galvanostatic polarization curve as the boundary conditions. But there was some agreement between the experimental measurement and the calculated galvanic current distribution using potentiostatic polarization curves obtained at a slow scan rate as the boundary conditions. The galvanostatic polarization curve of AZ91D did not represent the behavior of AZ91D because steady state had not been reached. The galvanic current decreased with exposure time which could be due to the gradual formation of a partially protective film. The potentiodynamic polarization curves at the lower scan rates were also consistent with this interpretation. The formation of a partially protective film is plausible in the coolant because the coolant does contain inhibitors designed to decrease the corrosion rate. The inhibitors are designed for non-Mg alloys, but may nevertheless have an inhibiting effect on Mg alloy [43, 44].

BEM can be used to predict the magnesium galvanic corrosion behavior in weakly corrosive environments (such as corrosive water) and inhibited environments (such as coolant) provided that an appropriate polarization curve is used. In both of the two solutions, steady state had not been reached, and for the coolant, the galvanostatic measurements lacked measured values at low current densities.

Conclusion

The BEM Model gave an adequate prediction of an AZ91D-steel couple provided the BEM model has as input an appropriate boundary condition. The BEM model requires a polarization curve that accurately reflects corrosion taking place. Provided the polarization curve reflects steady state, the BEM model is expected to reflect steady state galvanic corrosion.

Acknowledgements

The authors would like to acknowledge the financial support of the Cooperative Research Centre for Cast Metals Manufacturing (CAST). CAST was established and is funded in part by the Australian Government's Cooperative Research Centres Program.

Reference

1. Song, G.L. and A. Atrens, *Corrosion Mechanisms of Magnesium Alloys*. Advanced Engineering Materials, 1999. **1**(1): p. p11-33.
2. Song, G.L. and A. Atrens, *Understanding magnesium corrosion: a framework for improved alloy performance*. Advanced Engineering Materials, 2003. **5**(12): p. 837-858.
3. Song, G.L., Johannesson, B., Hapugoda, S., and StJohn, D.H., Galvanic corrosion of magnesium alloy AZ91D in contact with an aluminium alloy, steel and zinc. Corrosion Science, 2004. **46**(4): p. 955-977.
4. Teeple, H.O., *Atmospheric galvanic corrosion of magnesium coupled to other metals*. Am. Soc. Testing Materials, Spec. Tech. Publ., 1956. **No. 175**: p. 89-115.
5. Song, G.L., *Corrosion of Magnesium Alloys*, in *Dept. of Mining, Minerals and Materials Engineering*. 1997, the University of Queensland: Brisbane. p. 178.
6. Wu, X., *Study on Corrosion and protection of Magnesium Alloy*, in *Institute of Corrosion and Protection of Metals*. 1999, Chinese Academy of Science: Shenyang China. p. 89.
7. Skar, J.I., *Corrosion and corrosion prevention of magnesium alloys*. Materials and Corrosion-Werkstoffe Und Korrosion, 1999. **50**(1): p. 2-6.
8. Ghali, E., *Corrosion and protection of magnesium alloys*. Magnesium Alloys 2000, 2000. **350-3**: p. 261-272.

9. Baldwin, K.R., Bray, D. J., Howard, G. D., and Gardiner, R. W., Corrosion behaviour of some vapour deposited magnesium alloys. *Materials Science and Technology*, 1996. 12(11): p. 937-943.
10. Makar, G.L. and J. Kruger, *Corrosion of Magnesium*. International Materials Reviews, 1993. **38**(3): p. 138-153.
11. Olsen, A.L., *Corrosion Properties of New Magnesium Alloys*. Metall, 1992. **46**(6): p. 570-574.
12. Genesca, J., L. Betancourt, and C. Rodriguez, *Electrochemical behavior of a magnesium galvanic anode under ASTM test method G 97-89 conditions*. Corrosion, 1996. **52**(7): p. 502-507.
13. Kaese, V., Niemeyer, M., Tai, P., Rottger, J., Enhancing corrosion resistance of magnesium base-alloys by alloying Part 1: Dynamic alkalization of the boundary layer - Ternary alloys. *Materials and Corrosion-Werkstoffe Und Korrosion*, 1999. 50(4): p. 191-198.
14. Waber, J.T., *Study of a size effect in galvanic corrosion*. Corrosion, 1957. **13**: p. 95t-102t.
15. Wagner, C., *Theoretical analysis of the current density distribution in electrolytic cells*. J. Electrochem. Soc., 1951. **98**: p. 116-28.
16. Scully, J.R. and H.P. Hack, *Prediction of tube-tubesheet galvanic corrosion using finite element and Wagner number analyses*. ASTM Spec. Tech. Publ., 1988. **978**(Galvanic Corros.): p. 136-57.
17. Kucera, V., *Galvanic corrosion in the atmosphere*. Rapp. - Korrosionsinst., 1977(16): p. 43 pp.
18. Konig, F. and M. Papke, *Contact corrosion of aluminum/steel and magnesium/steel joints*. Mit Oberflaechentech. 21. Jahrhundert Kommun.-Verkehrstech., Berichtsband Ulmer Gespraech, 20th, 1998: p. 24-34.
19. Umehara, H., M. Takaya, and T. Itoh, *Atmospheric galvanic corrosion behavior of AZ91D coupled to other metals*. Keikin-zoku, 1999. **49**(4): p. 172-177.
20. Isacson, M., Strom, M., Rootzen, H., and Lunder, O., Galvanically induced atmospheric corrosion on magnesium alloys: a designed experiment evaluated by extreme value statistics and conventional techniques. Soc. Automot. Eng., [Spec. Publ.] SP, 1997. SP-1250(Characteristics and Applications of Magnesium in Automotive Design): p. 43-55.
21. Boese, E., Gollner, J., Heyn, A., Strunz, J., Baierl, C., and Schreckenberger, H., Galvanic corrosion behaviour of magnesium alloy in contact with coated components. *Materials and Corrosion-Werkstoffe Und Korrosion*, 2001. 52(4): p. 247-256.
22. Tahara, A. and T. Kodama, *Potential distribution measurement of galvanic corrosion by Kelvin probe*. Zairyo to Kankyo, 1998. **47**(6): p. 391-395.
23. Adey, R.A. and S.M. Niku, *Computer modeling of corrosion using the boundary element method*. ASTM Spec. Tech. Publ., 1992. **STP 1154**(Comput. Model. Corros.): p. 248-64.

24. Munn, R.S., *A review of the development of computational corrosion analysis for spatial corrosion modeling through its maturity in the mid-1980s*. ASTM Spec. Tech. Publ., 1992. **STP 1154**(Comput. Model. Corros.): p. 215-28.
25. Aoki, S. and K. Kishimoto, *Prediction of Galvanic Corrosion Rates by the Boundary Element Method*. Mathematical and Computer Modelling, 1991. **15**(3-5): p. 11-22.
26. Aoki, S., K. Kishimoto, and M. Miyasaka, *Analysis of potential and current density distributions using a boundary element method*. Corrosion (Houston), 1988. **44**(12): p. 926-32.
27. Brebbia, C.A. and S. Walker, *Boundary element in engineering*. 1979, Butterworth.
28. Jia, J.X., Song, G., Atrens, A., St.John, D., Baynham, J., and Chandler, G., *Evaluation Of The Beasy Program Using Linear And Piecewise Linear Approaches For The Boundary Conditions*. Materials and Corrosion-Werkstoffe Und Korrosion, 2004: p. in press.
29. Kishimoto, K., H. Miyasaka, and S. Aoki, *Boundary Element Analysis of an Inverse Problem in Galvanic Corrosion*. Jsme International Journal Series I- Solid Mechanics Strength of Materials, 1989. **32**(2): p. 256-262.
30. Miyasaka, M., Hashimoto, K., Kishimoto, K., and Aoki, S., *A Boundary Element Analysis on Galvanic Corrosion Problems - Computational Accuracy on Galvanic Fields with Screen Plates*. Corrosion Science, 1990. **30**(2-3): p. 299-311.
31. Fischer, W., U. Hermann, and M. Schroder, *Simulation of a Corrosion Element Consisting of a Coated Steel Electrode with a Damage*. Werkstoffe Und Korrosion-Materials and Corrosion, 1991. **42**(12): p. 620-625.
32. Varela, F.E., Y. Kurata, and N. Sanada, *The influence of temperature on the galvanic corrosion of a cast iron-stainless steel couple (prediction by boundary element method)*. Corrosion Science, 1997. **39**(4): p. 775-788.
33. Helle, H.P.E., G.H.M. Beek, and J.T. Ligtelijn, *Numerical determination of potential distributions and current densities in multielectrode systems*. Corrosion (Houston), 1981. **37**(9): p. 522-30.
34. Orazem, M.E., et al., *Mathematical models for cathodic protection of an underground pipeline with coating holidays: Part 1 - Theoretical development*. Corrosion (Houston), 1997. **53**(4): p. 264-272.
35. Strong, G.E., R.A. Adey, and R.S. Rudas, *Computer prediction of interference current corrosion*. Int. Corros. Congr., Proc., 13th, 1996: p. Paper 56/1-Paper 56/6.
36. Bardal, E., R. Johnsen, and P.O. Gartland, *Prediction of galvanic corrosion rates and distribution by means of calculation and experimental models*. Corrosion (Houston), 1984. **40**(12): p. 628-33.
37. Ault, J.P., Jr. and J.J. Meany, Jr., *A test of the reliability of mathematically modeling corrosion*. Corros. Control Low-Cost Reliab., Proc. - Int. Corros. Congr., 12th, 1993. **5A**: p. 3519-30.

38. Benbow, W.E., *Steels in modern industry : a comprehensive survey*. 1951., London :: Iron and Steel by Iliffe., 562p .:
39. ASTM, D1384, *STANDARD TEST METHOD FOR CORROSION TEST FOR ENGINE COOLANTS IN GLASSWARE*. 1996.
40. Hack, H.P. and J.R. Scully, *Galvanic Corrosion Prediction Using Long-Term and Short-Term Polarization Curves*. *Corrosion*, 1986. **42**(2): p. 79-90.
41. Oldfield, J.W., *Electrochemical theory of galvanic corrosion*. *Galvanic Corrosion*, ASTM STP 978., ed. H.P. Hack. 1988, Philadelphia: American Society for Testing and Materials. 5-22.
42. Hartt, W.H., C.H. Culberson, and S.W. Smith, *Calcareous deposits on metal surfaces in seawater - a critical review*. *Corrosion* (Houston, TX, United States), 1984. **40**(11): p. 609-18.
43. Song, G. and D. StJohn, *Corrosion of magnesium alloys in commercial engine coolants*. *Materials and Corrosion-Werkstoffe Und Korrosion*, 2005. **(in press)**.
44. Song, G. and D. StJohn, *Corrosion behaviour of magnesium in ethylene glycol*. *Corrosion Science*, 2004. **46**(6): p. 1381-1399.

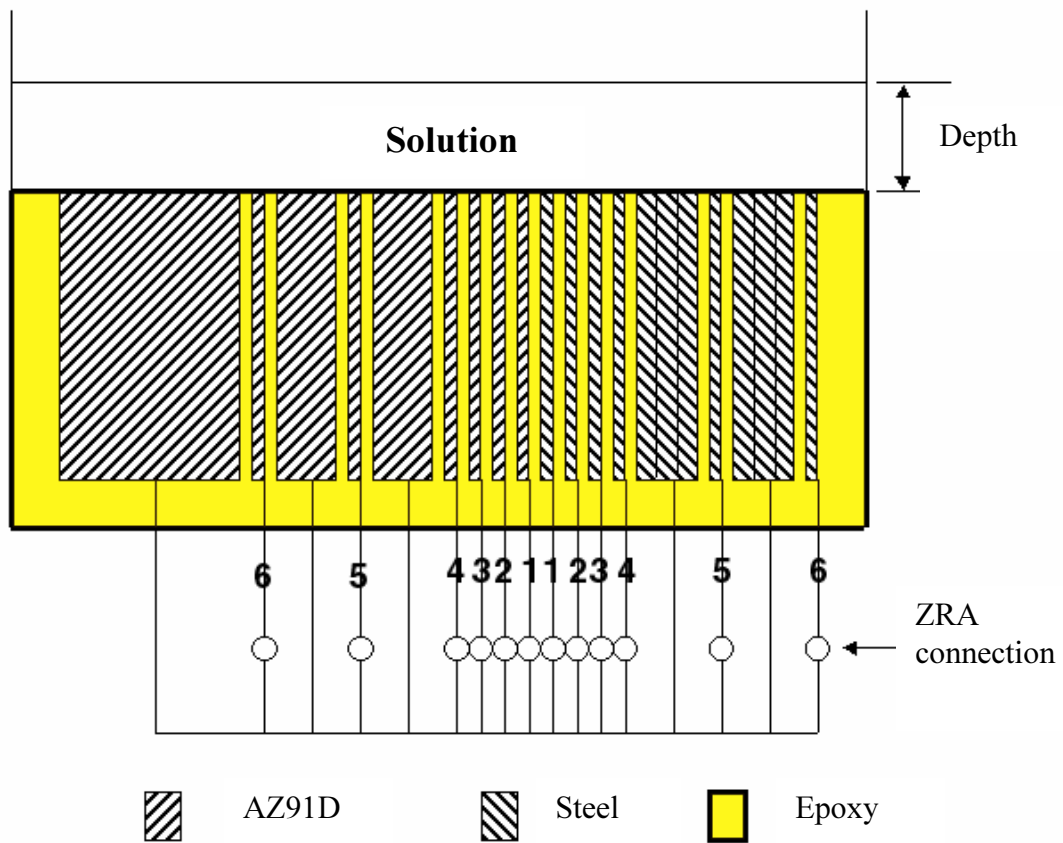


Figure 1. Schematic of multi-electrode Mg-steel galvanic corrosion assembly.

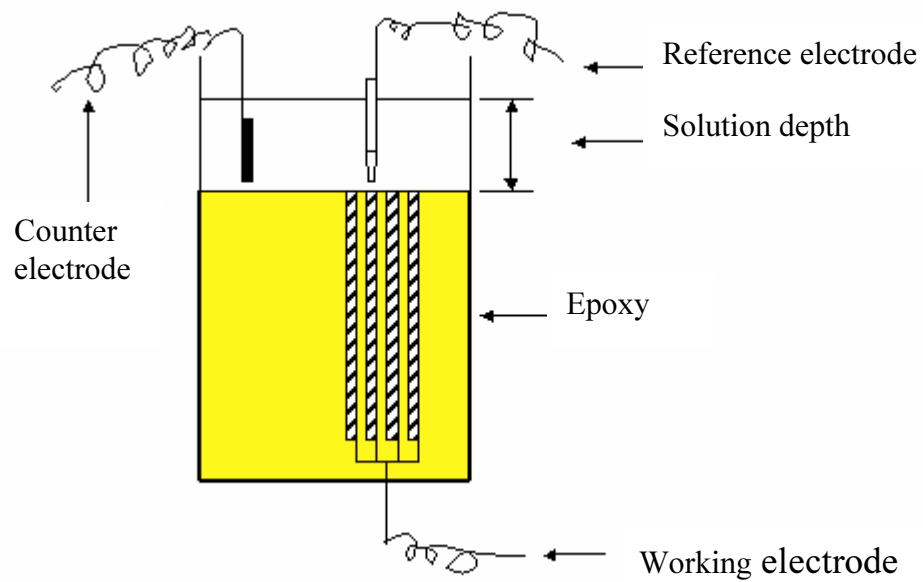


Figure 2. Schematic of arrangement for measuring polarization curves.

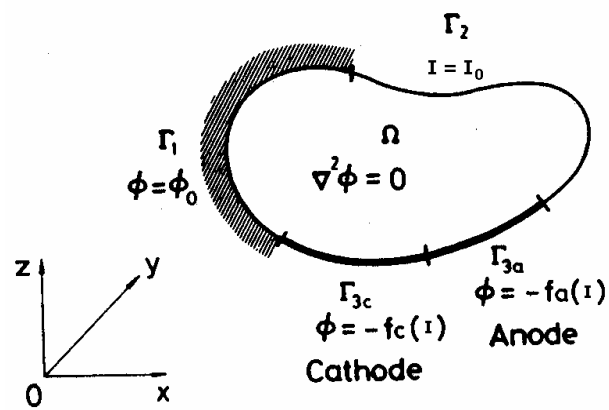


Figure 3. Basic equations and boundary conditions for the BEM model.

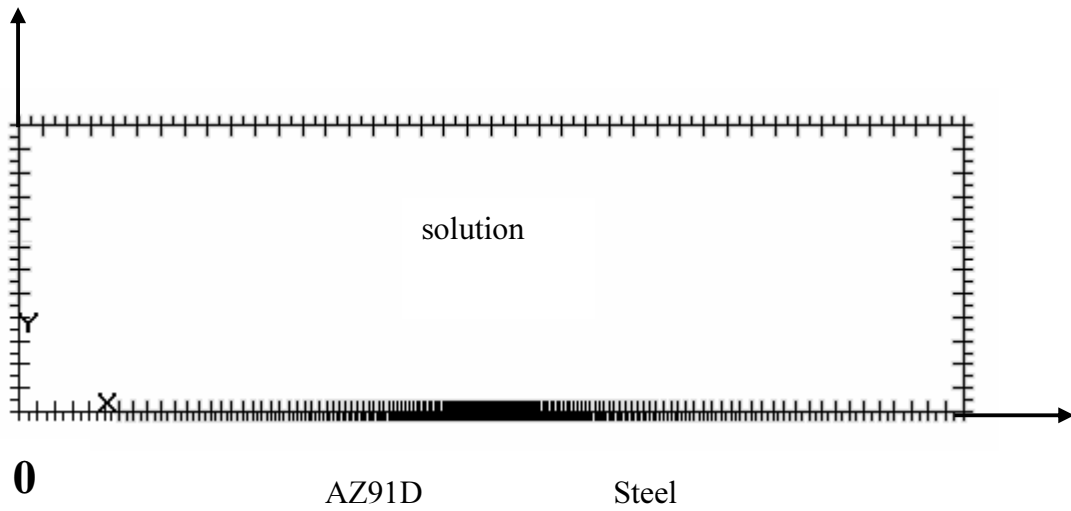


Figure 4. Schematic illustration of the detail of the BEM mesh for the geometry presented in figure 1.

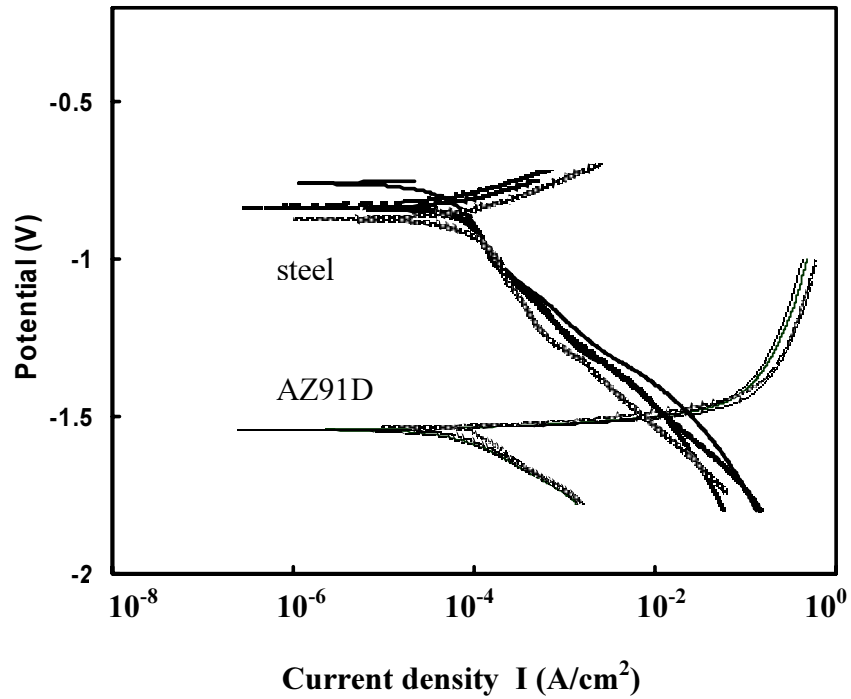


Figure 5. Potentiodynamic polarization curves for AZ91D and steel in 5% NaCl solution using a scan rate of 2mV/s. Solution depth was 10 mm.

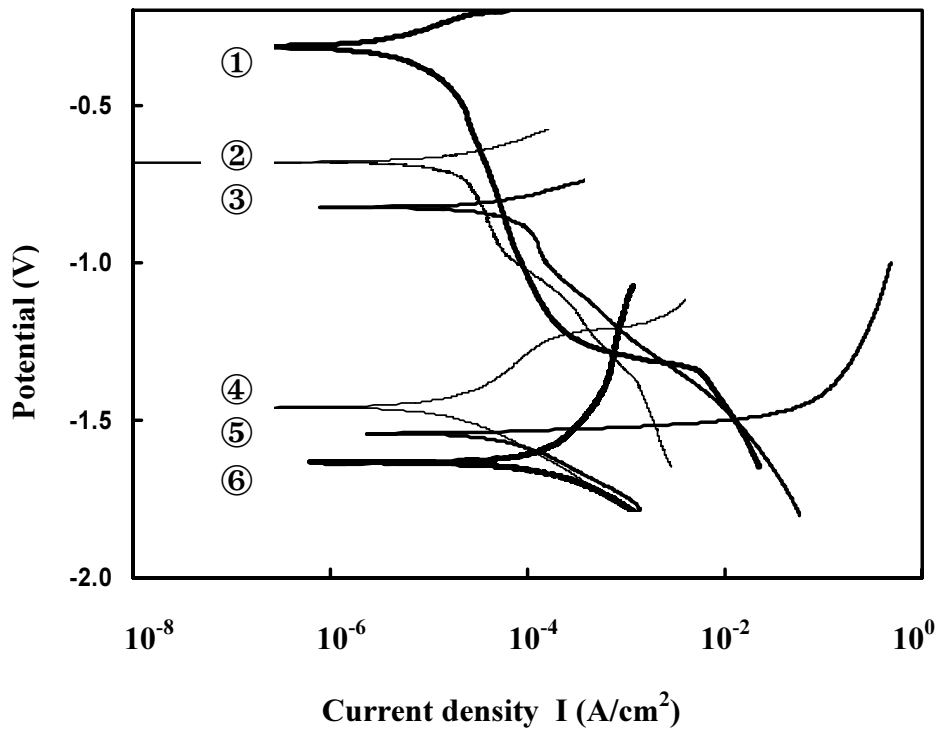


Figure 6. Typical potentiodynamic polarization curves at a scan rate of 2 mV/s in coolant (① for steel and ⑥ for AZ91D), corrosive water (② for steel and ④ for AZ91D) and 5% NaCl solution (③ for steel and ⑤ for AZ91D).

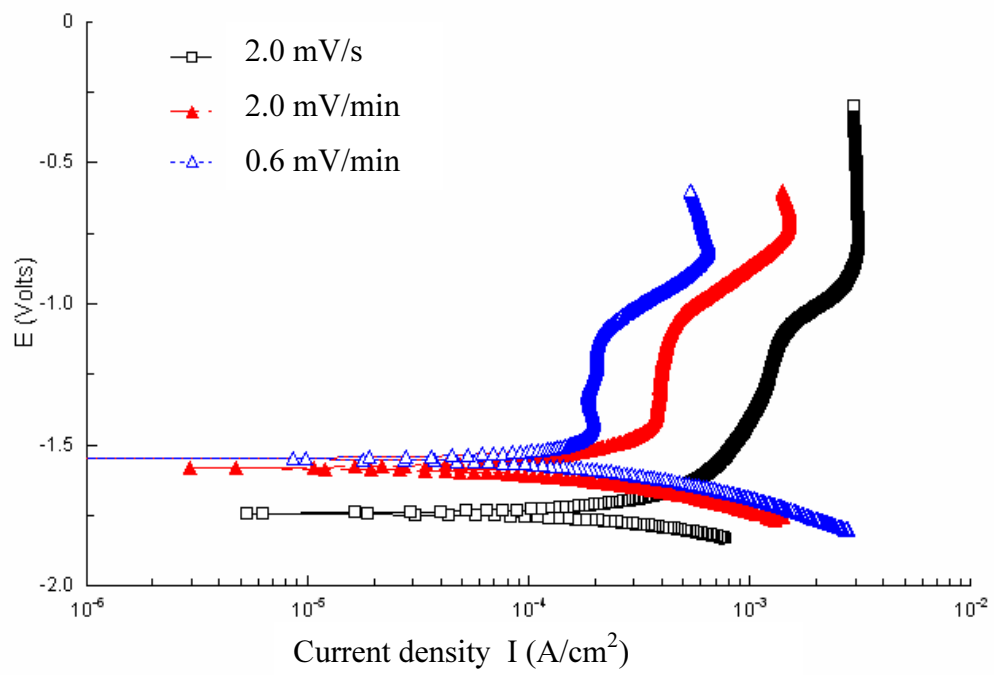


Figure 7. Potentiodynamic polarization curves with different potential scan rates for AZ91D in coolant.

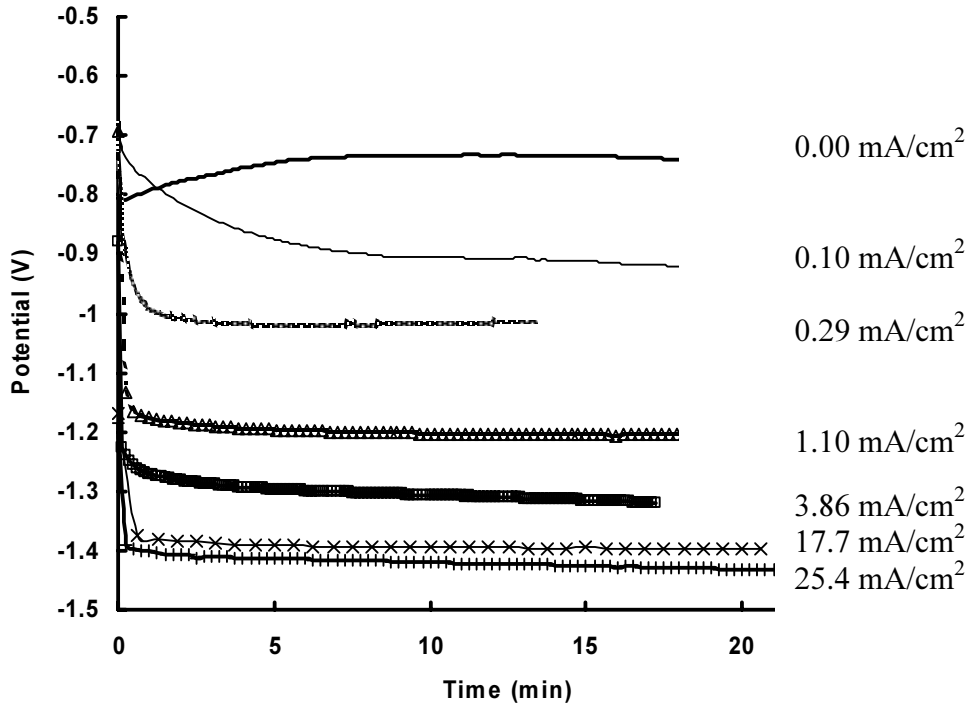


Figure 8. Galvanostatic measurement of potential versus time for steel in 5% NaCl solution at room temperature.

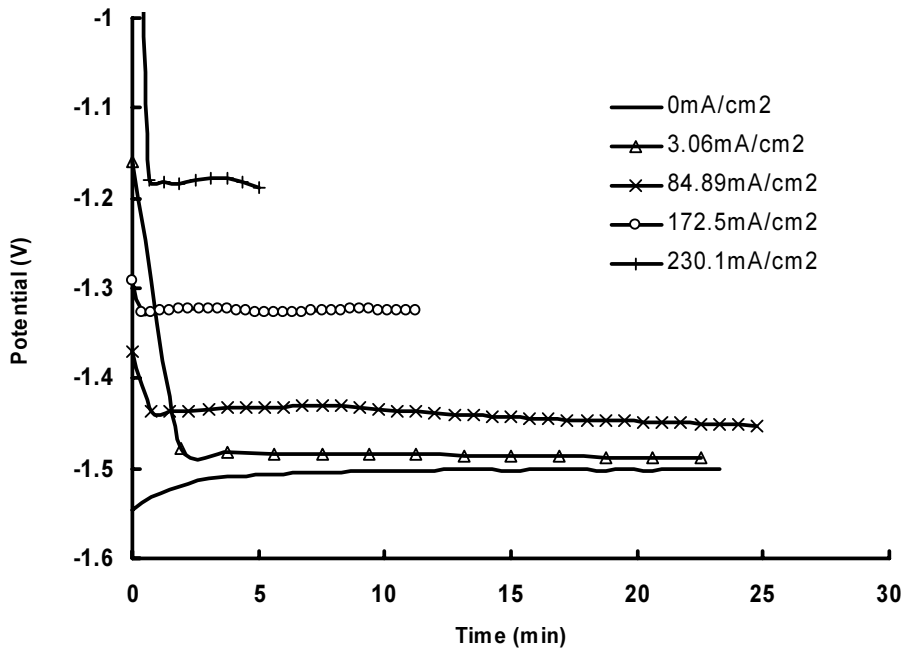


Figure 9. Galvanostatic measurement of potential versus time for AZ91D in 5% NaCl solution at room temperature.

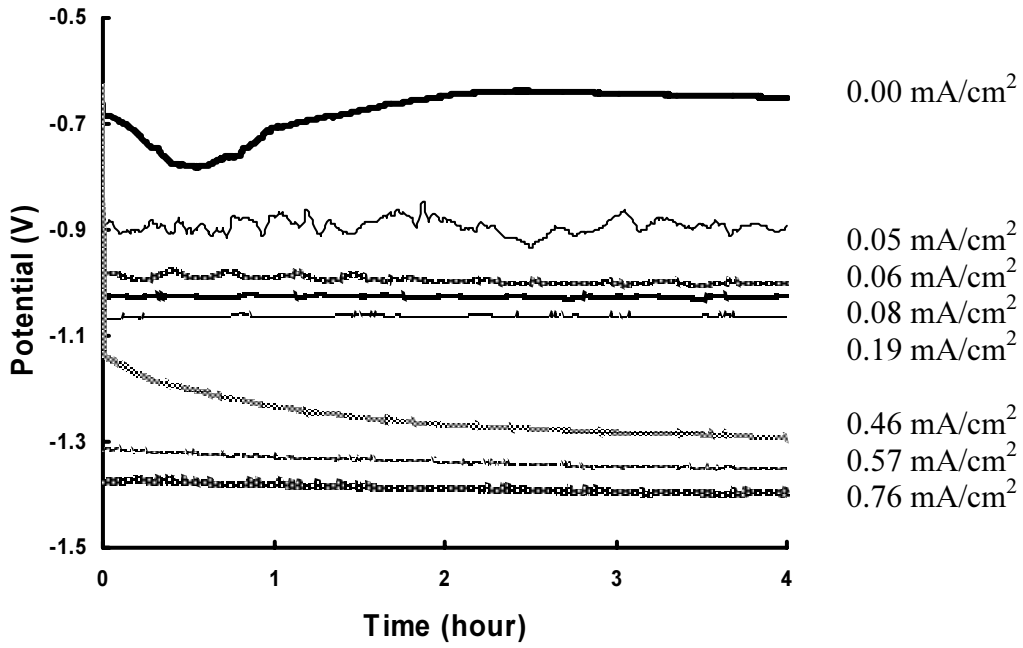


Figure 10. Galvanostatic measurement of potential versus time for steel in corrosive water at room temperature. The curves are in the order of the applied current density.

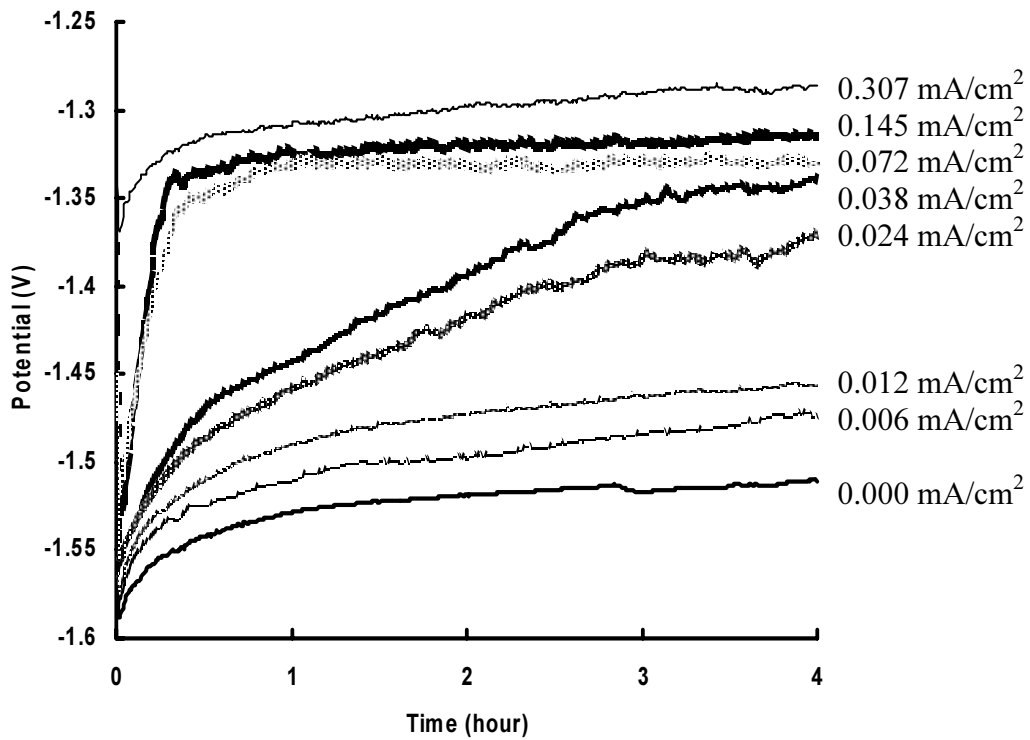


Figure 11. Galvanostatic measurement of potential versus time for AZ91D in corrosive water at room temperature. The curves are in the order of the applied current density.

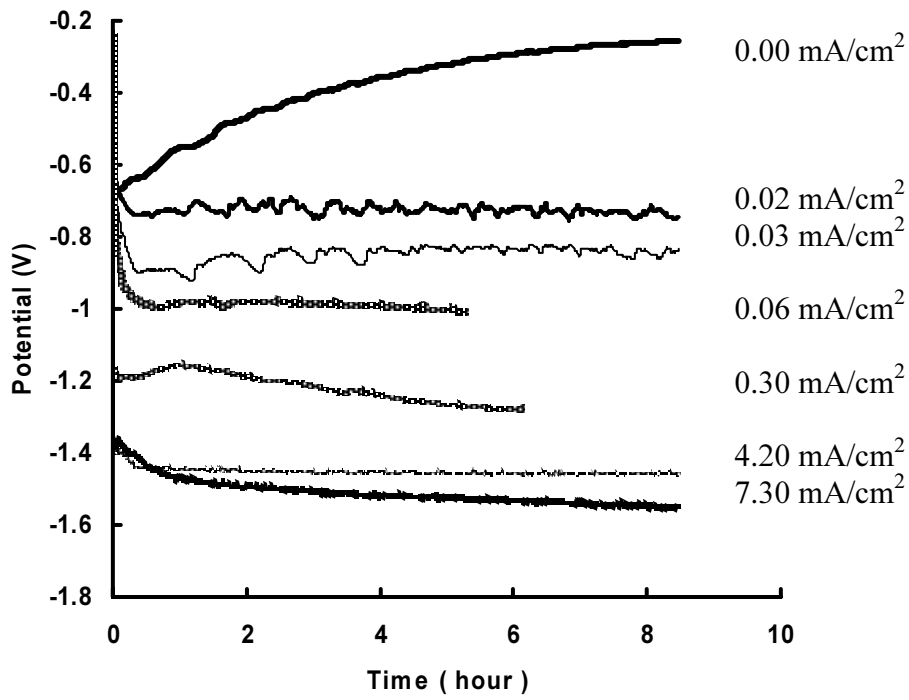


Figure 12. Galvanostatic measurement of potential versus time for steel in coolant at room temperature.

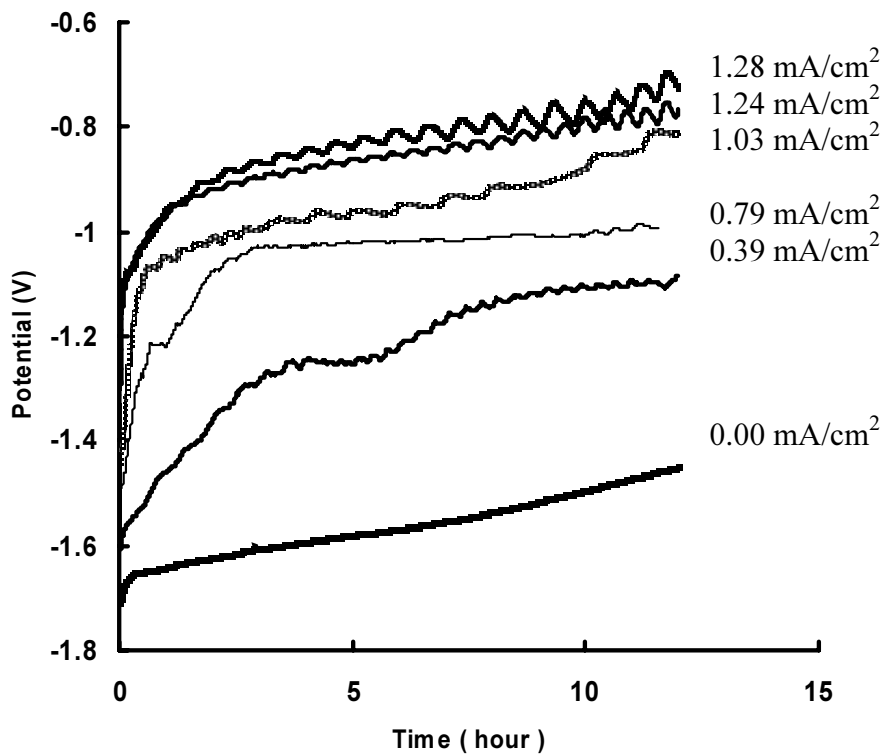


Figure 13. Galvanostatic measurement of potential versus time for AZ91D in coolant at room temperature.

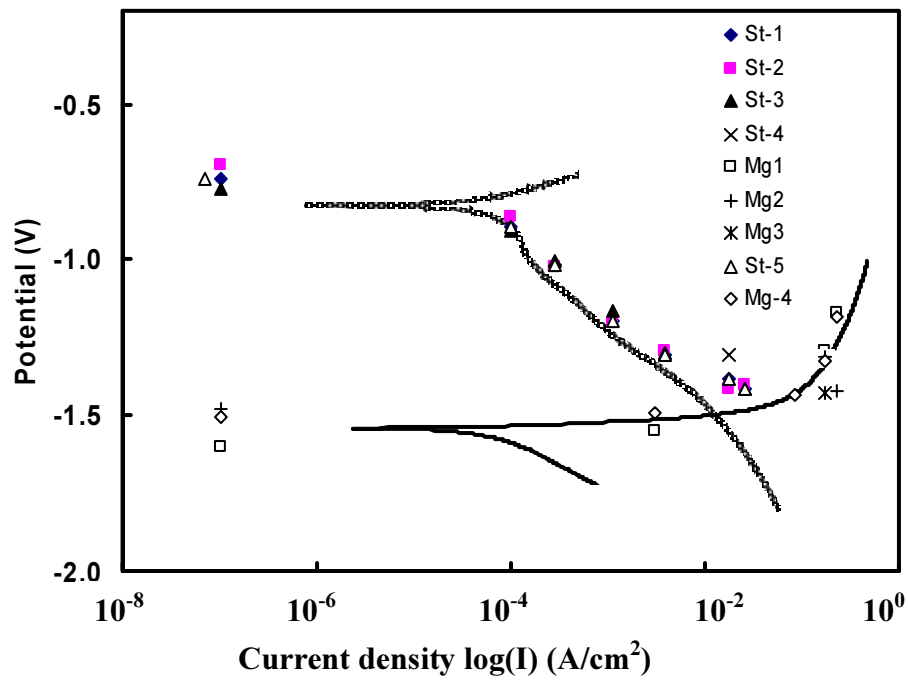


Figure 14. Galvanostatic polarization curve measurements in 5%NaCl solution. Curves represent typical potentiodynamic polarization curves, at scan rate of 2 mV/s.

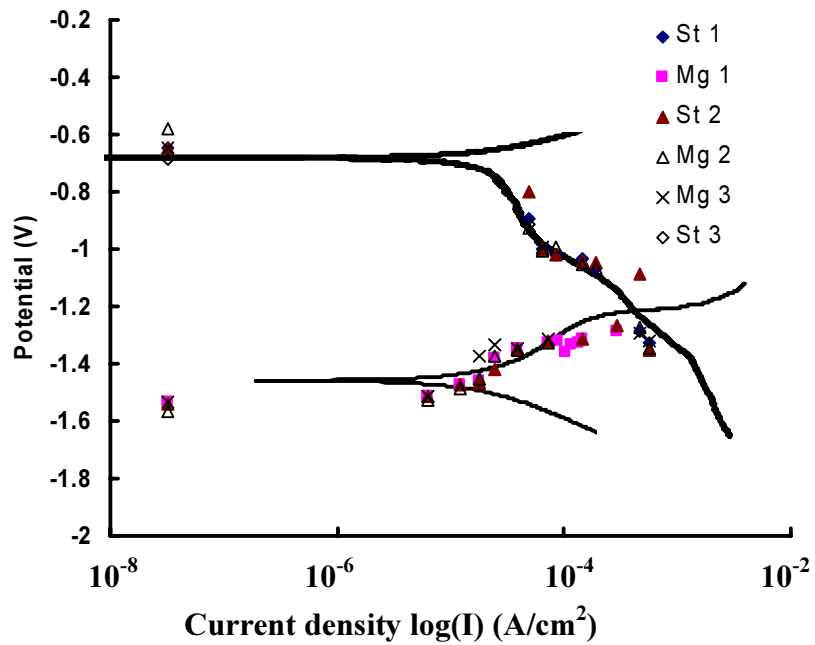


Figure 15. Galvanostatic polarization curve measurements in corrosive water. Curves represent typical potentiodynamic polarization curves, at a scan rate of 2 mV/s.

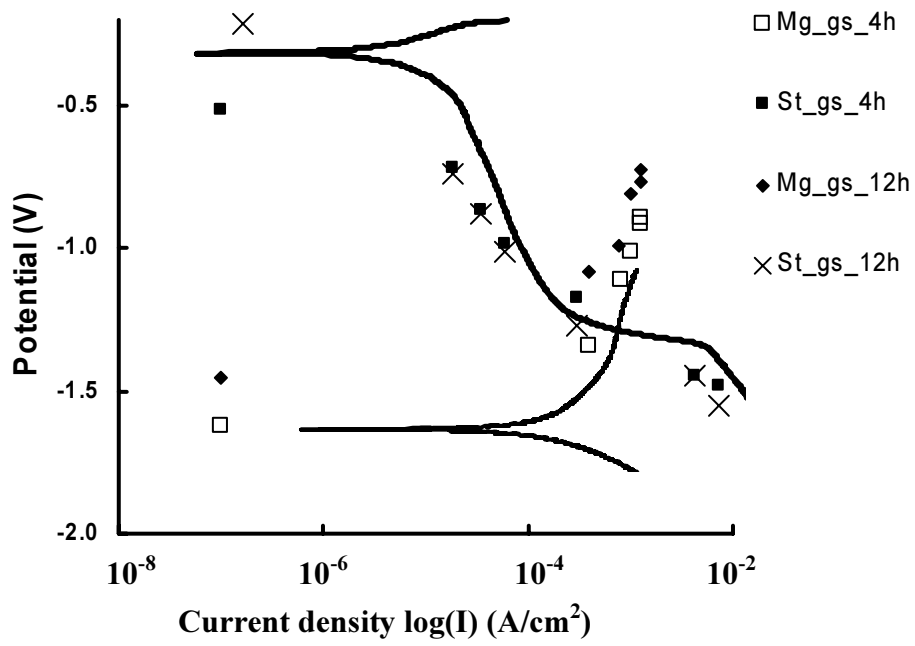


Figure 16. Galvanostatic polarization curve measurements in coolant. Curves represent typical potentiodynamic polarization curves at a scan rate of 2 mV/s.

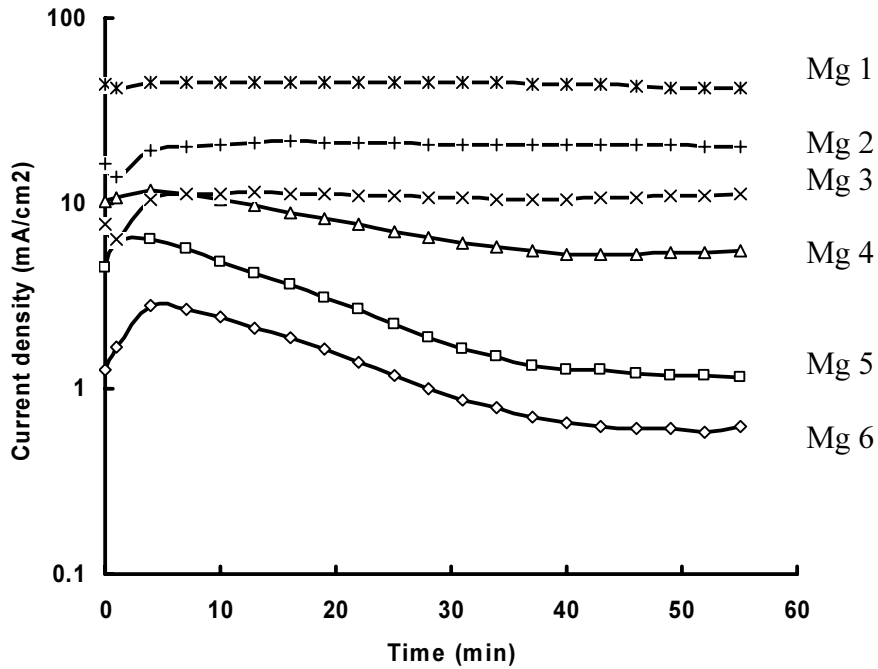


Figure 17. Galvanic current density at AZ91D electrodes (designated Mg 1 to Mg 6) in 5% NaCl solution.

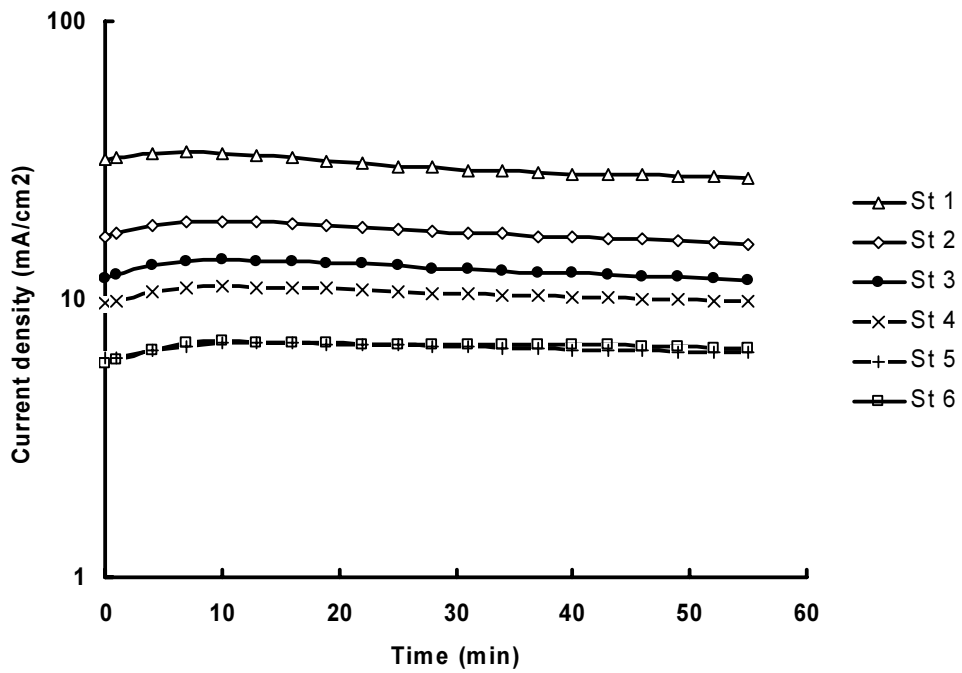


Figure 18. Galvanic current density at steel electrodes (designated St 1 to St 6) in 5% NaCl solution.

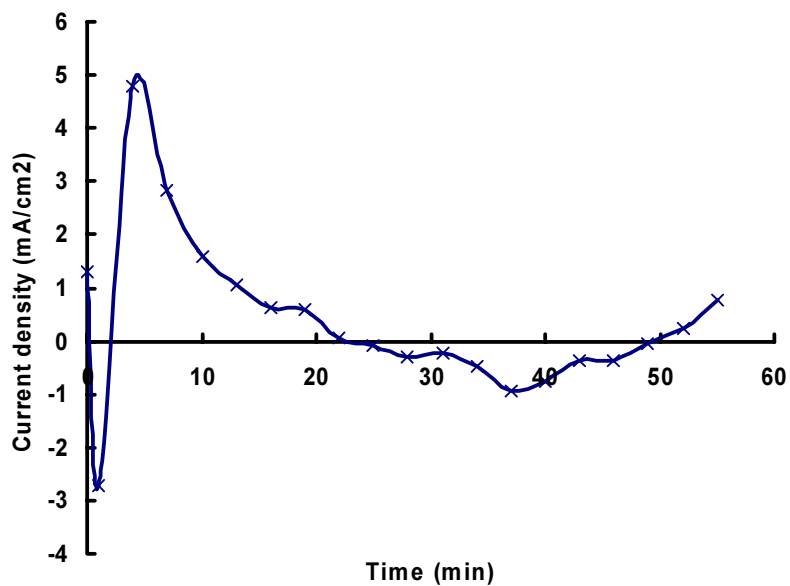


Figure 19. Sum of anode and cathode current in 5% NaCl solution.

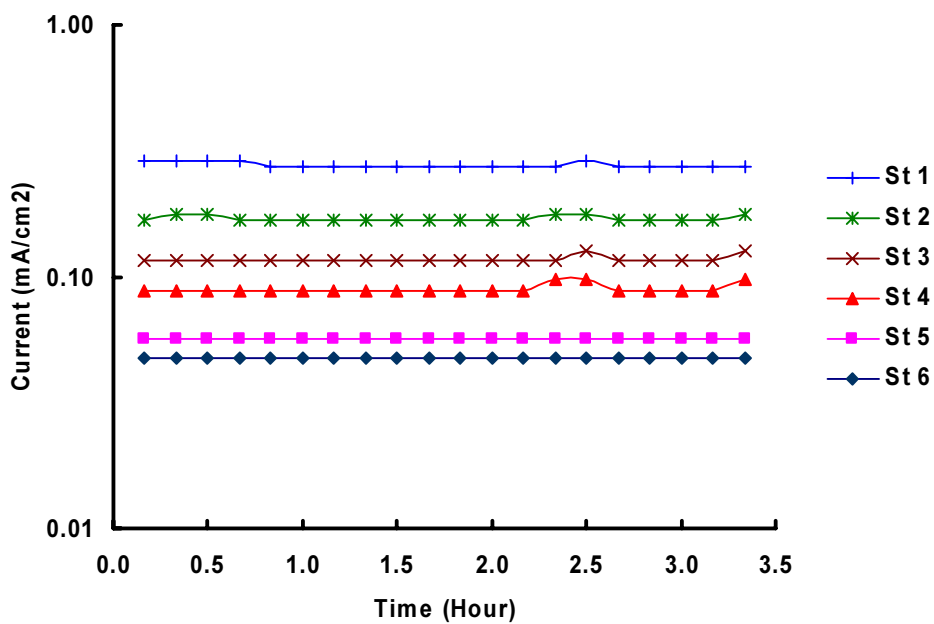


Figure 20. Galvanic current density for steel electrodes (designated St 1 to St 6) in corrosive water.

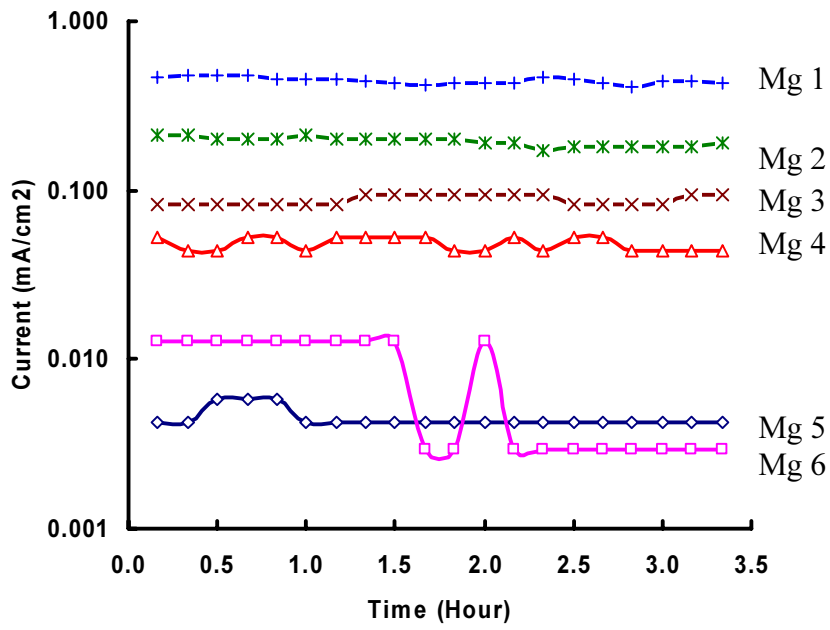


Figure 21. Galvanic current density for AZ91D electrodes (designated Mg 1 to Mg 6) in corrosive water.

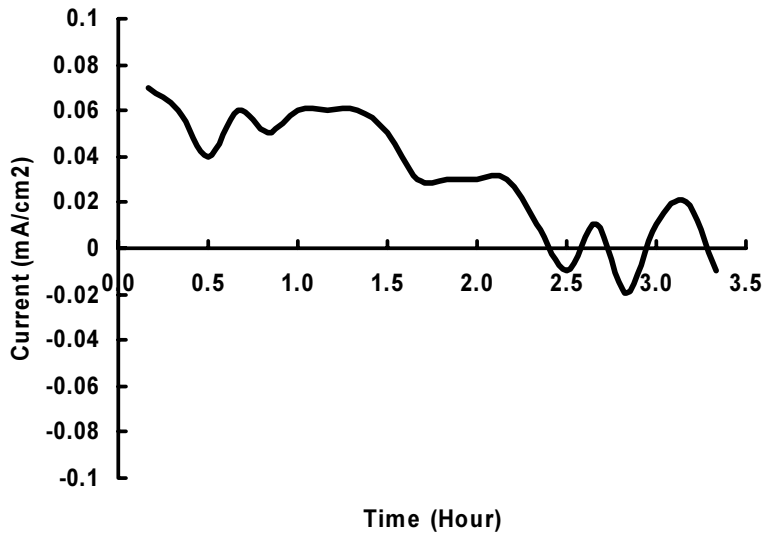


Figure 22. Sum of anode and cathode currents in corrosive water.

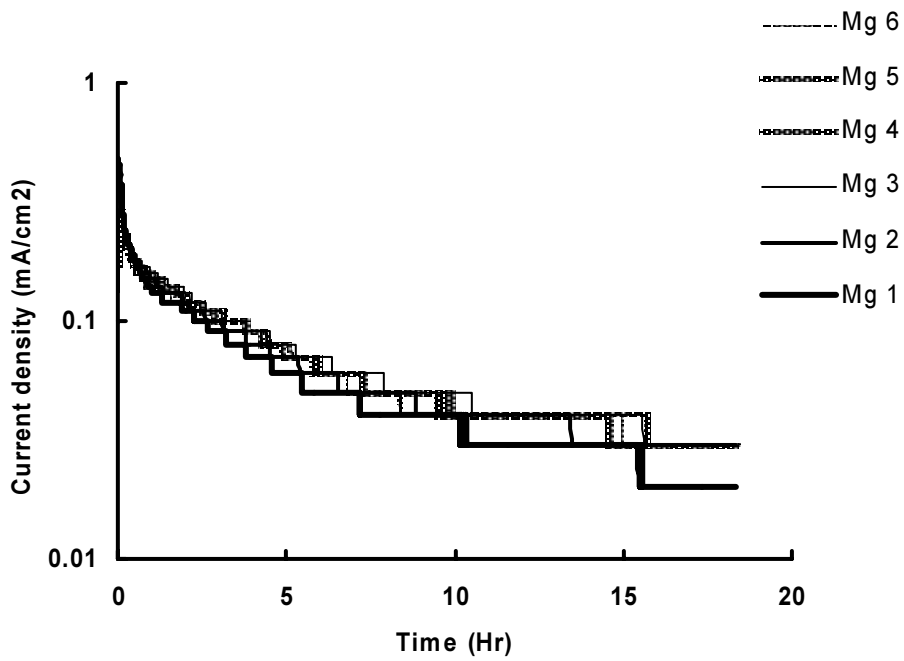


Figure 23. Galvanic current density at AZ91 electrodes (designated Mg 1 to Mg 6) in coolant.

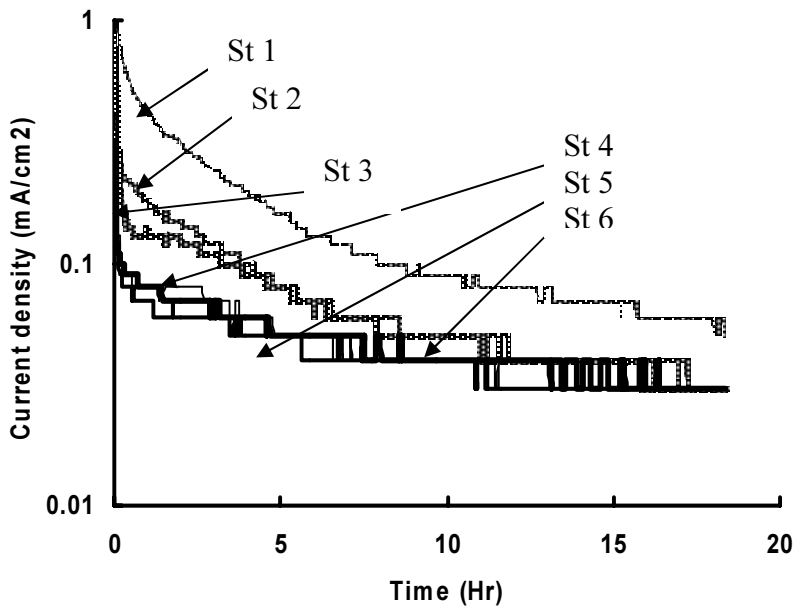


Figure 24. Galvanic current density at steel electrodes (designated St 1 to St 6) in coolant.

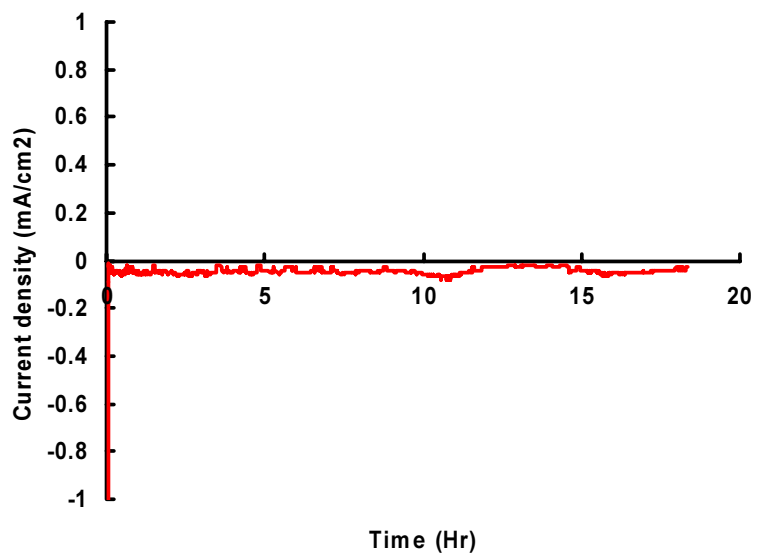


Figure 25. Sum of current from anode and cathode in coolant.

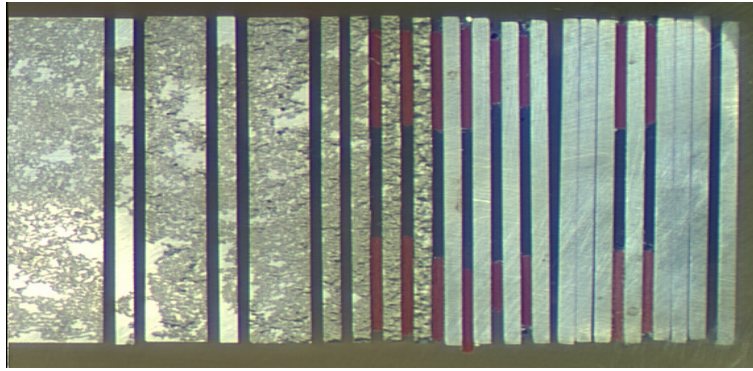


Figure 26. Surface appearance of AZ91D-steel couple after 30 minutes galvanic corrosion test in 5%NaCl solution. AZ91D is on the left.

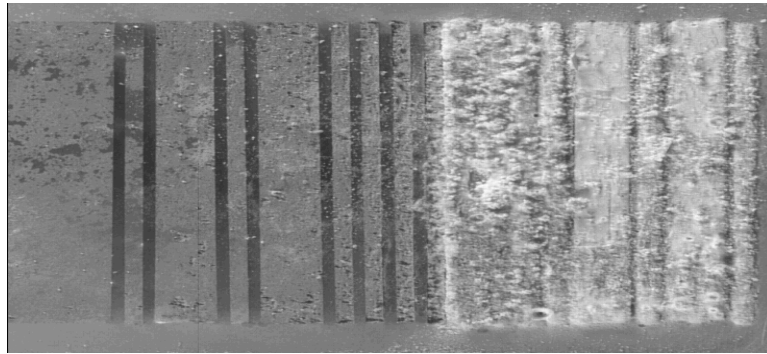


Figure 27. Surface appearance of AZ91D-steel couple after 20 hours galvanic corrosion test in corrosive water. AZ91D is on the left.

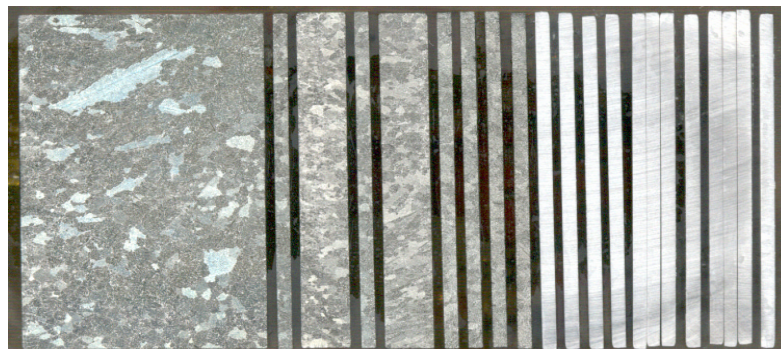


Figure 28. Surface appearance of AZ91D-steel couple after 20 hours galvanic corrosion test in coolant. AZ91D is on the left.

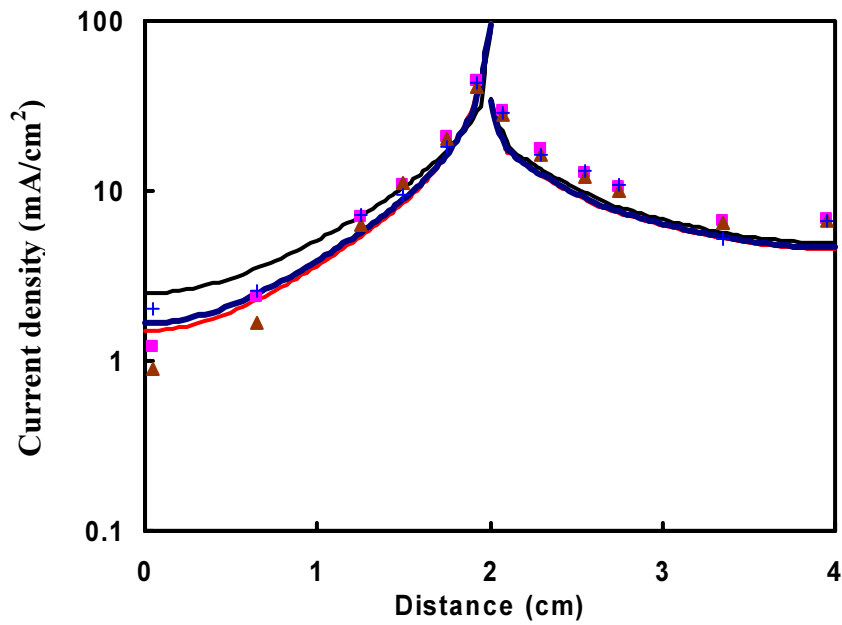


Figure 29. Comparison of experimental measurements of galvanic current density in 5% NaCl measured at 50 – 60 min (data points) and BEM calculation with different boundary conditions as specified in Table 1. Curves represent BEM calculations.

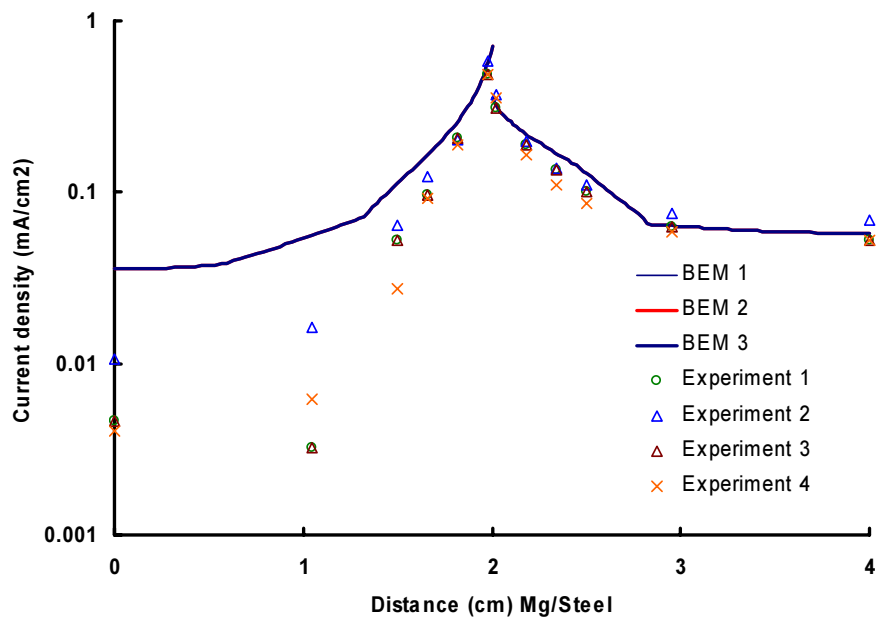


Figure 30. Comparison of experimental measurements of galvanic current density in corrosive water measured at ~3hr (data points) and BEM calculation with different boundary conditions as specified in Table 2. Curves represent BEM calculations.

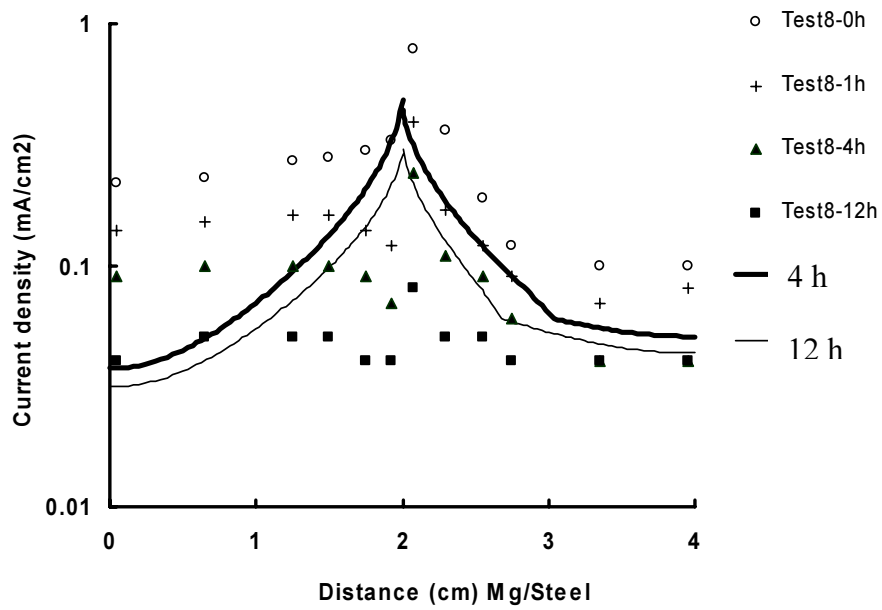


Figure 31. Comparison of BEASY predictions (curves) using the time dependent galvanostatic polarization curve and experimental measurements (data points) in coolant.

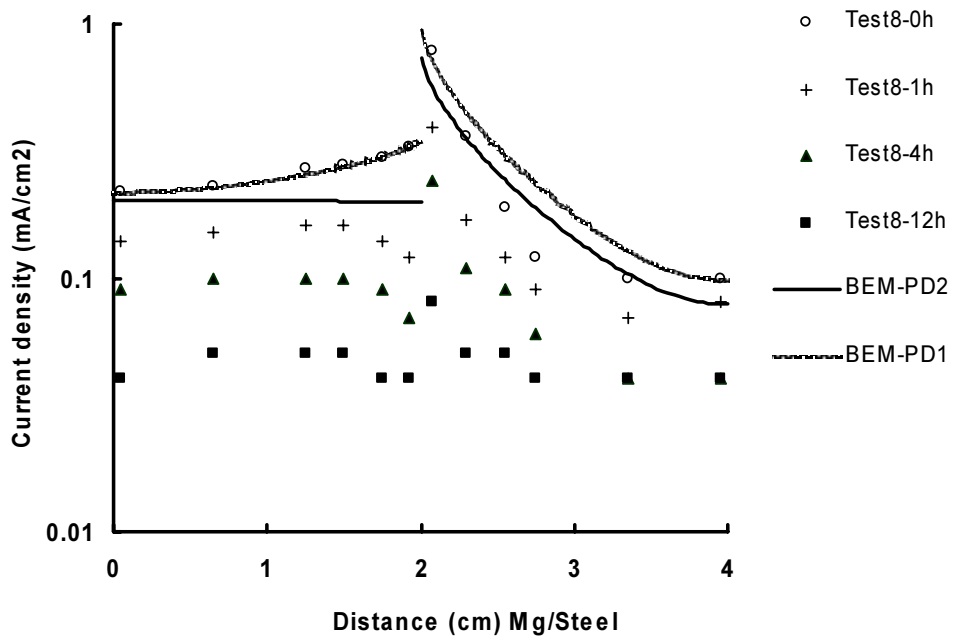


Figure 32. Comparison of BEASY predictions (curves) using potentiodynamic polarization curve as boundary condition and experimental measurements (data points) in coolant.

Table 1. Boundary conditions in 5% NaCl solution used for BEM calculations, related to the data of figure 14.

	Current density (mA/cm ²)	Potential (V)	Potential (V)	Potential (V)
		BEM 1	BEM 2	BEM 3
Steel	0.000	-0.771	-0.695	-0.741
	0.100	-0.906	-0.863	-0.896
	0.290	-1.003	-1.021	-1.018
	1.100	-1.165	-1.202	-1.194
	3.860	-1.298	-1.296	-1.305
	17.700	-1.307	-1.413	-1.386
	25.400	-1.418	-1.403	-1.417
AZ91D	0.000	-1.480	-1.600	-1.506
	-3.058	-1.430	-1.550	-1.492
	-84.880	-1.431	-1.431	-1.431
	-172.500	-1.310	-1.290	-1.325
	-230.100	-1.420	-1.170	-1.183

Table 2. Boundary conditions in corrosive water used for BEM calculations, related to the data of figure 15.

	Current density (mA/cm ²)	Potential (V)	Potential (V)	Potential (V)
		BEM 1	BEM 2	BEM 3
Steel	0.000	-0.644	-0.648	-0.578
	0.049	-0.895	-0.800	-0.927
	0.065	-1.002	-0.998	-1.005
	0.085	-1.018	-1.021	-1.021
	0.146	-1.036	-1.039	-1.055
	0.190	-1.066	-1.049	-1.068
	0.459	-1.290	-1.086	-1.273
	0.570	-1.328	-1.355	-1.345
AZ91D	0.000	-1.532	-1.538	-1.569
	-0.006	-1.512	-1.510	-1.524
	-0.012	-1.475	-1.474	-1.486
	-0.018	-1.457	-1.465	-1.455
	-0.024	-1.379	-1.419	-1.371
	-0.038	-1.348	-1.345	-1.352
	-0.072	-1.326	-1.320	-1.328
	-0.145	-1.315	-1.310	-1.316
	-0.288	-1.288	-1.268	-1.268